Focus on molecular imaging: Gilad and colleagues provide an introduction to MRI reporter genes, which have the unique advantage of offering gene expression information that can be coregistered with anatomic and functional data. . . . ***Page 1905***

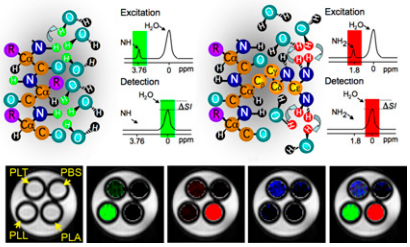

Exploring resolved chest pain: Dilsizian looks at current evidence about and imaging approaches to metabolic change after transient episodes of myocardial ischemia and previews a related article in this issue of *JNM*. . . . . ***Page 1909***

Dual-tracer PET/CT in HCC: Park and colleagues evaluate the addition of ^{11}C-acetate to ^{18}F-FDG PET/CT in the detection of primary and metastatic hepatocellular carcinoma. . . . . ***Page 1912***

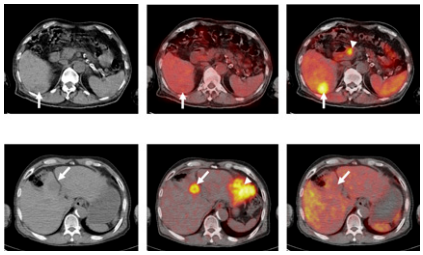

Identifying elevated OEF: Hokari and colleagues report on a methodology designed to improve the validity of acetazolamide testing for elevated oxygen extraction fraction in assessment for subsequent ischemic stroke. . . . . ***Page 1922***

PET in specific cancers: Hillner and colleagues expand on their previous report of aggregate data from the National Oncologic PET Registry by detailing results for specific cancer types and indications for testing. . . . . ***Page 1928***

PET and recurrent cervical cancer: van der Veldt and colleagues investigate the clinical value of ^{18}F-FDG PET in clarification of diagnosis and enhancement of management in suspected recurrence of cervical cancer. . . . . ***Page 1936***

Novel PET hypoxia tracer: Komar and colleagues explore the utility of ^{18}F-EF5, one of a new group of etanidazole-based compounds, in PET/CT imaging of hypoxia in patients with squamous cell carcinoma of the head and neck. . . . . ***Page 1944***

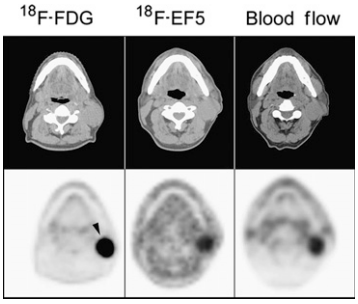

^{131}I SPECT/CT in thyroid cancer: Chen and colleagues compare the relative merits of ^{131}I SPECT/CT and whole-body scintigraphy in the management of patients with differentiated thyroid carcinoma. . . . . ***Page 1952***

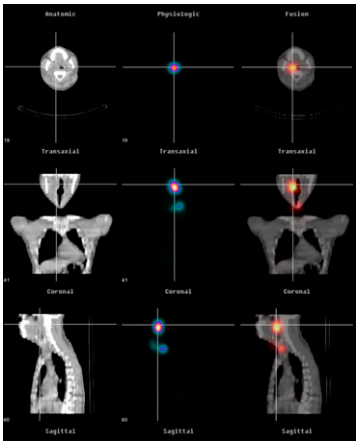

CAD in bone scans: Sadik and colleagues describe the development of an automated system for computer-assisted interpretation of whole-body bone scans performed to determine the presence or absence of metastases. . . . . ***Page 1958***

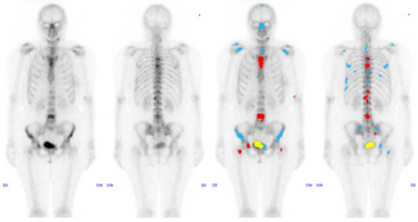

MAP kinase and NIS function: Jung and colleagues investigate the role of mitogen-activated protein kinase–linked signaling on the regulation of sodium/iodide symporter function in cancer cells and discuss the resulting implications for radioiodide therapy. . . . . ***Page 1966***

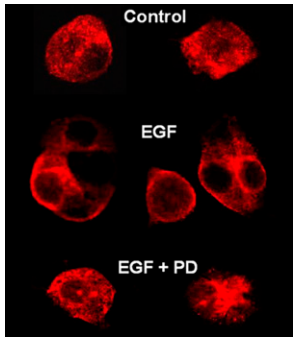

Heterogeneity in sarcoma: Eary and colleagues report on a study designed to determine whether heterogeneity in ^{18}F-FDG spatial distribution on PET can be used to predict tumor biologic aggressiveness and patient outcomes. . . . ***Page 1973***

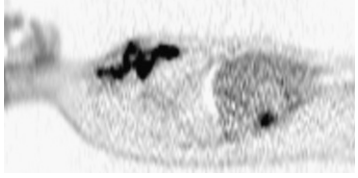

PET/CT in FUO: Keidar and colleagues evaluate the role of ^{18}F-FDG in the investigation of fever of unknown origin and review the potential of this technique for initial noninvasive clinical assessment. . ***Page 1980***

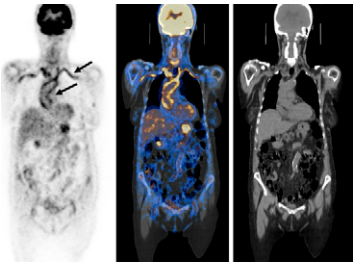

Persistent uptake after exercise: Dou and colleagues explore whether increased regional myocardial ^{18}F-FDG uptake in patients with coronary artery disease persists in rest imaging 24 h after an episode of exercise-induced myocardial ischemia. . . . ***Page 1986***

Attenuation correction of ^{82}Rb PET/CT: Slomka and colleagues compare transmission CT–based and CT-based attenuation for myocardial perfusion PET/CT images. . . . . ***Page 1992***

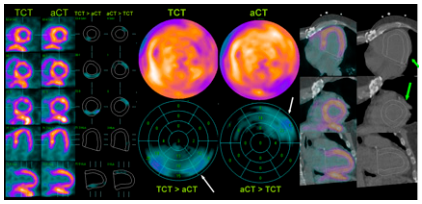

Brain metabolism in HIV and drug use: Georgiou and colleagues use ^{18}F-FDG PET to investigate both the separate and coexisting effects of HIV-1 infection and injected drug use on brain metabolic processes.. . . . . ***Page 1999***

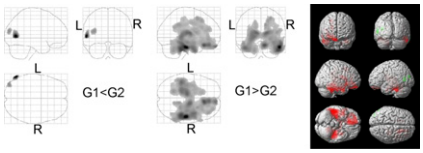

Neural substrates of Parkinson's dementia: Lee and colleagues investigate changes in cerebral glucose metabolism after cholinesterase inhibitor therapy in patients with Parkinson's disease dementia to determine whether cognitive improvements are reflected in changes of cerebral metabolic patterns. . . ***Page 2006***

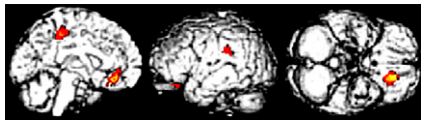

SPECT/CT in primary hyperparathyroidism: Neumann and colleagues compare the diagnostic accuracy of ^{99m}Tc-sestamibi/^{123}I subtraction SPECT with SPECT/CT for preoperative localization of abnormal parathyroid glands in patients with primary hyperparathyroidism. . . . . ***Page 2012***

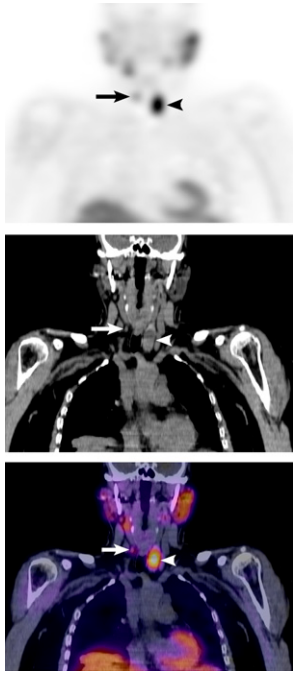

Kinetic modeling of ^{11}C-HOMADAM: Nye and colleagues report on a reliable model describing healthy human brain uptake kinetics for this novel PET radioligand with high affinity and selectivity for the serotonin transporter. . . . . ***Page 2018***

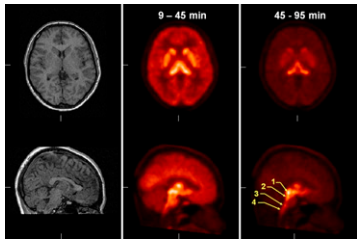

Radioimmunotherapy for Graves disease: Eterović and colleagues evaluate the effects of self-absorption of ^{131}I radiation in the follicular colloid on the absorbed dose to thyroid follicular cells. . . . . ***Page 2026***

Novel prostate cancer tracers: Apolo and colleagues provide an educational overview of current molecular imaging modalities that have been clinically tested in metastatic prostate cancer, including consideration of conformity with current prostate cancer clinical trial designs. . . . . ***Page 2031***

mGluR5 receptors in human brain: Brown and colleagues explore the characteristics and potential of ^{18}F-SP203, a novel PET radioligand for metabotropic glutamate subtype 5 receptors, in healthy human brains. ***Page 2042***

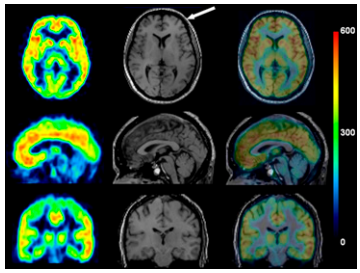

Cytotoxicity of σ-ligands: Rybczynska and colleagues quantify receptor occupancies associated with the cytotoxic effect of σ-ligands and assess dose-dependent changes of cellular metabolism in a tumor cell line. . ***Page 2049***

^{18}F-FLT kinetics in mice: Kim and colleagues describe a kinetic modeling analysis method for quantitative ^{18}F-FLT PET proliferation imaging in subcutaneous tumor models in mice.. . . . . ***Page 2057***

ON THE COVER

Regional myocardial ^{18}F-FDG uptake is highly specific and sensitive for exercise-induced myocardial ischemia and may persist for 24 h after an episode. Exercise and rest ^{99m}Tc-sestamibi perfusion and ^{18}F-FDG imaging were performed on this patient with exertional angina. Exercise-induced perfusion abnormality was reversible on rest images, and intense ^{18}F-FDG uptake on exercise images was not seen on rest images. The patient had 85% right coronary artery stenosis.

See page 1989.